Symmetrized-basis LASTO calculations of defects in CdTe and ZnTe

Yia-Chung Chang
Department of Physics and Materials Research Laboratory, University of Illinois at Urbana-Champaign, 1110 West Green Street, Urbana, Illinois 61801, USA

R. B. James and J. W. Davenport
Brookhaven National Lab, Upton, New York 11973-5000, USA
(Received 7 May 2005; revised manuscript received 4 November 2005; published 23 January 2006)

The electronic structures of defects (vacancies and donor-vacancy pair) in CdTe and ZnTe are studied with a full-potential linearized augmented Slater-type orbital (LASTO) code. A symmetrized basis is constructed, which improves the computation efficiency of the LASTO code by two orders of magnitude when applied to large supercells with high point symmetry. Thus, we can model defects in CdTe via a large supercell (up to 128 atoms) with only modest computation effort. The lattice relaxation, the formation energy, and the energy position of defect levels for various charged states are determined. The theoretical results are compared with available experimental data and previous theoretical studies.

DOI: 10.1103/PhysRevB.73.035211 PACS number(s): 61.72.Vv, 71.55.Gs, 61.72.Ji

I. INTRODUCTION

$Cd_{1-x}Zn_xTe$ (CZT) is an important material for radiation detectors.[1] One of the extrinsic factors that degrades the usefulness of the material is the carrier trapping by native defects which are present during the growth. The most dominant defects in CZT are believed to be Cd vacancies, interstitials, and the related defect complexes such as halogen-vacancy pairs. Thus, it is highly desirable to have a better understanding of the electronic properties of these defects. Extensive experimental studies of defects in CdTe have been reported.[2–8] There also exist a number of theoretical studies.[9–14] Berding *et al.* performed linear-muffin-tin-orbital (LMTO) calculations of the formation energy of Cd vacancies in CdTe.[6,7] Meijer *et al.*[11] examined the energy levels of neutral as well as charged Cd vacancies with an empirical tight-binding model. Biernacki *et al.*[12] studied the Cd-vacancy—Cl pair in CdTe also with a tight-binding model. Wei and Zhang studied the chemical trend of defect formation and doping limit in CdTe within the linearized augmented-plane-wave (LAPW) method.[13] However, many important details such as the effects of atomic relaxation and the spin-orbit interaction on various charge states of the defect remain largely unexplored. In this paper, we perform *ab initio* calculations of the electronic structures of Cd vacancies and Cd-Cl pair in CdTe and Zn vacancies in ZnTe with a full-potential linearized augmented Slater-type orbital (LASTO) method,[14–16] taking into account the effects of atomic relaxation and the spin-orbit interaction on the defect levels. Our studies provide some insight into the nature of various defect-induced states. For large supercells (e.g., 128 atoms), only one **k** point is sufficient for determining the total energy. With the choice of $\mathbf{k}=\mathbf{0}$, the system is invariant under the full point-group of the crystal. Thus, the application of point group theory can drastically reduce the computation effort. The idea of using symmetrized basis to study defects was adopted by Kirton *et al.*[18] They have applied this scheme to vacancies in GaP and ZnSe with a plane-wave pseudopotential method with good success. In this paper we describe the implementation of symmetrized basis for the full potential LASTO code and apply this method to determine the energy positions of the defect levels associated with Cd and Zn vacancies by using supercells of 54 and 128 atoms. We find that this implementation improves the computation efficiency by two orders of magnitude for supercells with size larger than 32 atoms.

II. THEORETICAL METHOD

Our *ab initio* calculations of the electronic structures of defects in CdTe and ZnTe are based on the full potential linearized augmented Slater-type orbital method developed by Davenport and co-workers.[14–17] The local density approximation (LDA) is used. To study the defect levels, we adopt a "supercell model," in which the system is viewed as a three-dimensional crystal (superlattice) with a large unit cell (supercell). The defect (Cd vacancy or interstitial) is placed at the center (an atomic or interstitial site) of a supercell, which contains 54, 64, or 128 atoms. The 64-atom supercell is a simple cube with the length of each side being $2a$ (a is the lattice constant of the host semiconductor). The 54- and 128-atom supercells have a shape of a rhombic dodecahedron (Wigner-Seitz cell of a fcc lattice) as shown in Fig. 1. The intervacancy distance is $\sqrt{4.5}a$, $2a$, and $\sqrt{8}a$, for the 54-, 64-, and 128-atom supercells, respectively. It is worth noting that the intervacancy distance in the 54-atom supercell is larger than that in the 64-atom supercell, even though the number of atoms enclosed is smaller. Thus, it is more advantageous to use the 54-atom supercell over the 64-atom supercell for modeling defects. The self-consistent calculation is first performed without the spin-orbit interaction to obtain the initial atomic relaxation and charge density. The self-consistent calculation including the spin-orbit interaction is then performed to fine-tune the relaxed positions of atoms surrounding the vacancy and the corrections to the energy levels are investigated. For a large supercell, the interaction between defects of two adjacent supercells becomes negli-

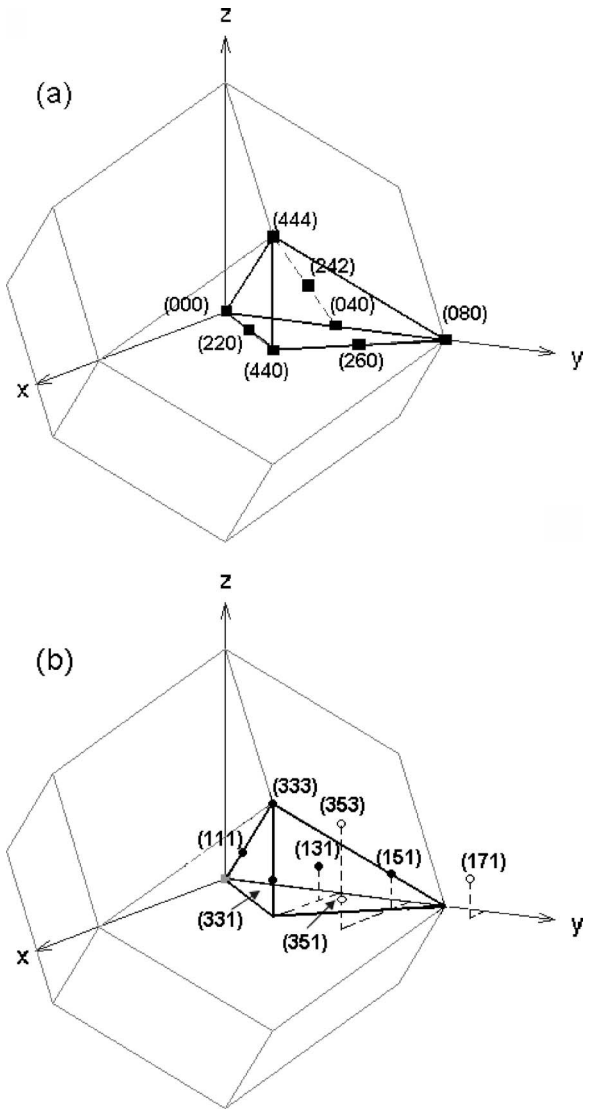

FIG. 1. (a) Wigner-Seitz cell of a 128-atom supercell. The solid squares indicate the positions of cations in the irreducible segment of the Wigner-Seitz cell. The coordinates are in units of $a/4$. (b) Wigner-Seitz cell of a 54-atom supercell. The solid circles indicate the positions of anions in the irreducible segment of the Wigner-Seitz cell. The open circles indicate the positions of anions outside the irreducible segment of the 54-atom supercell but within the irreducible segment of the 128-atom supercell.

gible, and the effect of band dispersion of the defect-related states of the superlattice can be ignored. Thus, we only need to consider the zone-center states (i.e., $\mathbf{k}=0$). In this case, the point-group symmetry of the system is preserved, and we can substantially reduce the computation effort by using symmetrized basis functions which transform according to the irreducible representations of of point group. For doubly charged Cd vacancies, the dangling bonds are fully occupied. Thus, there is no Jahn-Teller distortion, and the point group remains the same as the host crystal, which is Td. For neutral and singly charged Cd vacancies and for Cd-Cl pair, trigonal, or tetragonal Jahn-Teller distortions are possible, and the corresponding point groups reduce to C_{3v} and D_{2d}.

The LASTO method was first introduced by Davenport and co-workers.[14–16] A full potential version was later implemented by Fernando *et al.*[17] Here we only give a brief account of the theory. A LASTO basis function at a given site (taken as the origin) is defined as

$$\psi_N(\mathbf{r}) = r^{n-1} e^{-\zeta_{nl} r} Y_{lm}(\hat{r}) \tag{1}$$

for $\mathbf{r}$ outside muffin-tin (MT) spheres and

$$\psi_N(\mathbf{r}) = \sum_{\tilde{N}} [\beta_{N\tilde{N}} g_{\tilde{l}}(r_{\tilde{i}}) + \alpha_{N\tilde{N}} \dot{g}_{\tilde{l}}(r_{\tilde{i}})] Y_{\tilde{l}\tilde{m}}(\hat{r}_{\tilde{i}}) \tag{2}$$

for $\mathbf{r}$ inside the MT sphere, where N is a composite index for the LASTO orbitals, which includes the site index i and orbital index $\{nlm\}$, while $\tilde{N}$ is a composite index for $\{\tilde{i},\tilde{l},\tilde{m}\}$, which labels the spherical harmonics expansion of the basis function at site $\tilde{i}$. ζ_{nl} denotes the exponents for the Slater-type functions, $r_{\tilde{i}}=|\mathbf{r}-\mathbf{R}_{\tilde{i}}|$, and $Y_{lm}(\hat{r}_{\tilde{i}})$ is the spherical harmonics centered at site $\mathbf{R}_{\tilde{i}}$. $g_{\tilde{l}}(r_{\tilde{i}})$ is the numerical solutions to the Kohn-Sham equation within the MT sphere at site $\mathbf{R}_{\tilde{i}}$ and $\dot{g}_{\tilde{l}}(r_{\tilde{i}})=(d/d\epsilon)g_{\tilde{l}}(r_{\tilde{i}})$ denotes the energy derivative of $g_{\tilde{l}}$. $\beta_{N\tilde{N}}$ and $\alpha_{N\tilde{N}}$ are structure coefficients that are determined by requiring the basis functions, and their derivatives are continuous across all MT-sphere boundaries including the tail contributions from LASTO basis functions from all other unit cells.

The most time consuming part of the LASTO code is the evaluation of the structure coefficients (α and β) and the overlap (S) and Hamiltonian (H) matrices, which involve double summation over the reciprocal lattice vectors $\mathbf{G}$ and $\mathbf{G}'$.[15] For $\mathbf{k}=0$ these matrices are given by

$$S_{N,N'} = \sum_{\tilde{N}} (\beta^*_{N\tilde{N}}\beta_{N'\tilde{N}} + \alpha^*_{N\tilde{N}}\alpha_{N'\tilde{N}}\langle \dot{g}_{\tilde{l}}|\dot{g}_{\tilde{l}}\rangle) + \frac{1}{v_s}\sum_{\mathbf{G}} \psi^*_N(\mathbf{G})\psi_{N'}(\mathbf{G}) - \frac{1}{v_s^2}\sum_{\mathbf{G},\mathbf{G}'} \psi^*_N(\mathbf{G})\psi_{N'}(\mathbf{G}')\sum_{\tilde{N}} e^{i(\mathbf{G}'-\mathbf{G})\cdot\mathbf{R}_{\tilde{i}}} f(|\mathbf{G}'-\mathbf{G}|), \tag{3}$$

$$H_{N,N'} = \epsilon\sum_{\tilde{N}} (\beta^*_{N\tilde{N}}\beta_{N'\tilde{N}} + \alpha^*_{N\tilde{N}}\alpha_{N'\tilde{N}}\langle \dot{g}_{\tilde{l}}|\dot{g}_{\tilde{l}}\rangle) + \frac{1}{v_s}\sum_{\mathbf{G}} \psi^*_N(\mathbf{G})(|\mathbf{G}|^2 + V_0)\psi_{N'}(\mathbf{G}) + \frac{1}{2}R_s^2\sum_{\tilde{N}} [g'_{\tilde{l}}\dot{g}_{\tilde{l}}(\beta^*_{N\tilde{N}}\alpha_{N'\tilde{N}} + \alpha^*_{N\tilde{N}}\beta_{N'\tilde{N}}) + g_{\tilde{l}}\dot{g}'_{\tilde{l}}\beta^*_{N\tilde{N}}\beta_{N'\tilde{N}} + \dot{g}'_{\tilde{l}}\dot{g}_{\tilde{l}}\alpha^*_{N\tilde{N}}\alpha_{N'\tilde{N}}] - \frac{1}{v_s^2}\sum_{\mathbf{G},\mathbf{G}'} \psi^*_N(\mathbf{G})\psi_{N'}(\mathbf{G}')\sum_{\tilde{N}} e^{i(\mathbf{G}'-\mathbf{G})\cdot\mathbf{R}_{\tilde{i}}}[\mathbf{G}\cdot\mathbf{G}' + V_0] f(|\mathbf{G}'-\mathbf{G}|), \tag{4}$$

where $f(|\mathbf{G}|)$ is the Fourier transform of the step function $\theta(r_s-|\mathbf{r}|)$, v_s is the supercell volume, and $\psi_N(\mathbf{G})$ is the Fourier transform of the LASTO orbital, $\psi_N(\mathbf{r}-\mathbf{r}_i)$. V_0 is the muffin-tin zero. $g_{\tilde{l}}$, $\dot{g}_{\tilde{l}}$, and $g'_{\tilde{l}} \equiv dg_{\tilde{l}}/dr$ appearing above are evaluated at $r=R_s$ (the muffin-tin radius). $\langle \dot{g}_{\tilde{l}}|\dot{g}_{\tilde{l}}\rangle \equiv \int dr r^2 \dot{g}_{\tilde{l}}(r)\dot{g}_{\tilde{l}}(r)$. To improve the computation efficiency we redefined the LASTO basis functions in terms of real spherical harmonics, $\mathcal{Y}_{lm}$. We define a real LASTO basis function as

$$\phi_N(\mathbf{r}) = r^{n-1}e^{-\zeta_{nl}r}\mathcal{Y}_{lm}(\hat{r}), \tag{5}$$

where

$$\mathcal{Y}_{lm}(\hat{r}) = \sqrt{2}ReY_{lm}(\hat{r}) \quad \text{for } m > 0, \tag{6}$$

$$\mathcal{Y}_{lm}(\hat{r}) = \sqrt{2}ImY_{lm}(\hat{r}) \quad \text{for } m < 0, \tag{7}$$

and $\mathcal{Y}_{l0}(\hat{r}) = Y_{l0}(\hat{r})$. Because $\phi_N(\mathbf{r})$ is real, its Fourier transform satisfies the relation $\phi_N(-\mathbf{q}) = \phi_N^*(\mathbf{q})$. $\beta_{N\tilde{N}}$ and $\alpha_{N\tilde{N}}$ are determined by the equations

$$\beta_{N\tilde{N}}g_{\tilde{l}} + \alpha_{N\tilde{N}}\dot{g}_{\tilde{l}},$$

$$= \sum_{\mathbf{G}} i^{\tilde{l}}F(Gr)\mathcal{Y}_{\tilde{l}\tilde{m}}(\hat{G})\phi_N(\mathbf{G})e^{-i\mathbf{G}\cdot\mathbf{r}_{\tilde{i}}} \equiv \sum_{\mathbf{G}} \mathcal{F}_{\tilde{N}}(\mathbf{G})\phi_N(\mathbf{G}), \tag{8}$$

and the corresponding equation for the energy derivative, where

$$F(Gr) = \frac{N_c}{v}{}_s 4\pi j_{\tilde{l}}(Gr), \tag{9}$$

and N_c is a normalization constant. Using the symmetry property of the spherical harmonics,

$$\mathcal{Y}_{\tilde{l}\tilde{m}}(-\hat{G}) = (-1)^{\tilde{l}}\mathcal{Y}_{\tilde{l}\tilde{m}}(\hat{G}), \tag{10}$$

we have

$$\mathcal{F}_{\tilde{N}}(-\mathbf{G}) = \mathcal{F}_{\tilde{N}}^*(\mathbf{G}). \tag{11}$$

Thus, $\beta_{N\tilde{N}}$ and $\alpha_{N\tilde{N}}$ are real. We can therefore rewrite the right-hand side of Eq. (8) as

$$\beta_{N\tilde{N}}g_{\tilde{l}} + \alpha_{N\tilde{N}}\dot{g}_{\tilde{l}} = \mathrm{Re}\sum_{\mathbf{G}}^{h} w(\mathbf{G})\mathcal{F}_{\tilde{N}}(\mathbf{G})\phi_N(\mathbf{G}), \tag{12}$$

where the superscript h means that the summation over $\mathbf{G}$ is carried out in the half space of $\mathbf{G}$. $w(\mathbf{G})$ is a weighting factor, which equals to 1 for $\mathbf{G}=0$ and 2 otherwise.

The double $\mathbf{G}$ sums appearing in Eqs. (3) and (4) contain terms like

$$T_n(\mathbf{G},\mathbf{r}_{N'}) \equiv \sum_{\mathbf{G}'} \phi_{N'}(\mathbf{G}')\mathcal{S}_n(\mathbf{G}',\mathbf{G}), \tag{13}$$

where

$$\mathcal{S}_n(\mathbf{G}',\mathbf{G}) = \sum_{\tilde{N}} e^{i(\mathbf{G}'-\mathbf{G})\cdot\mathbf{r}_{\tilde{i}}}f(|\mathbf{G}'-\mathbf{G}|)(\mathbf{G}'\cdot\mathbf{G})^n, \tag{14}$$

with $n=0$ or 1. It can be shown that $T_n(-\mathbf{G}) = T_n^*(\mathbf{G})$. Thus, we have

$$\sum_{\mathbf{G}} \phi_N^*(\mathbf{G})T_n(\mathbf{G}) = \mathrm{Re}\sum_{\mathbf{G}}^{h} w(\mathbf{G})\phi_N^*(\mathbf{G})T_n(\mathbf{G}). \tag{15}$$

A. Symmetrized basis according to point-group operations

Next, we consider the symmetrization which utilizes the point-group operations. We take linear combinations of the basis functions $\phi_N(\mathbf{r}-\mathbf{r}_\mathbf{i})$ for all $\mathbf{r}_i$ linked by the point-group operations such that it transforms like the νth partner of the irreducible representation Γ of the point group. We write

$$\psi_{\nu,s}^{\Gamma}(\mathbf{r}) = \sum_N C_{\nu,s}^{\Gamma}(N)\phi_N(\mathbf{r}-\mathbf{r}_\mathbf{i}), \tag{16}$$

where $\mathbf{r}_i$ runs through all atoms in a given shell, ν labels the degenerate partner functions, and $C_{\nu,s}^{\Gamma}(N)$ denotes the symmetrization coefficient, which can be generated using the group theory. The numerical procedures for obtaining $C_{\nu}^{\Gamma}(N)$ are described in the Appendix . We shall call $\psi_{\nu,s}^{\Gamma}(\mathbf{r})$ the shell orbitals. The extra index s labels different shell orbitals of the same symmetry type $(\Gamma\nu)$. The corresponding Fourier transform is denoted

$$\psi_{\nu,s}^{\Gamma}(\mathbf{G}) = \sum_N C_{\nu,s}^{\Gamma}(N)\phi_N(\mathbf{G}), \tag{17}$$

which shall replace $\phi_N(\mathbf{G})$ in Eqs. (8)–(15). Similarly, we define

$$\mathcal{F}_{\nu,\tilde{s}}^{\Gamma}(\mathbf{G}) = \sum_N C_{\nu,\tilde{s}}^{\Gamma}(N)\mathcal{F}_N(\mathbf{G}). \tag{18}$$

Equation (8) reduces to

$$\beta_{s,\tilde{s}}g_{\tilde{l}} + \alpha_{s,\tilde{s}}\dot{g}_{\tilde{l}} = \mathrm{Re}\sum_{\Lambda}\sum_{\mathbf{G}}^{r} [w(\Lambda\mathbf{G})/n_\Gamma]\psi_{\nu,s}^{\Gamma}(\Lambda\mathbf{G})\mathcal{F}_{\nu,\tilde{s}}^{\Gamma}(\Lambda\mathbf{G}), \tag{19}$$

where we have divided the half space of $\mathbf{G}$ into irreducible segments, which are related to one another by the point-group operations labeled by Λ. Here the superscript r indicates that the summation is carried out in the irreducible segment of the Brillouin zone only. Using the symmetry transformation

$$\psi_{\nu,s}^{\Gamma}(\Lambda\mathbf{G}) = \sum_{\nu'} \Gamma_{\nu,\nu'}(\Lambda)\psi_{\nu',s}^{\Gamma}(\mathbf{G}), \tag{20}$$

and similarly for $\mathcal{F}_{\nu,\tilde{s}}^{\Gamma}(\Lambda\mathbf{G})$, where $\Gamma_{\nu,\nu'}(\Lambda)$ are the matrix elements of the irreducible representation Γ for the group element Λ, we obtain

$$\beta_{s,\tilde{s}}g_{\tilde{l}} + \alpha_{s,\tilde{s}}\dot{g}_{\tilde{l}} = \mathrm{Re}\sum_{\nu'}\sum_{\mathbf{G}}^{r} [n(G^*)/n_\Gamma]\psi_{\nu',s}^{\Gamma}(\mathbf{G})\mathcal{F}_{\nu',\tilde{s}}^{\Gamma}(\mathbf{G}), \tag{21}$$

where $n(G^*)$ is the number of $\mathbf{G}$ vectors in the star of $\mathbf{G}$. In deriving the above relation, we have used the grand orthogonality theorem

$$\sum_{\Lambda} \Gamma_{\nu,\nu'}(\Lambda)\Gamma_{\nu,\nu''}(\Lambda) = n_h\delta_{\nu,\nu''}. \tag{22}$$

Here n_h is the order of the point group.

Because states of different symmetry types do not couple, S and H are block diagonalized, each block being associated with one symmetry type. Both indices N and N' in Eqs. (3) and (4) are now replaced by indices s and s' for shell orbitals. We have

$$T^{\Gamma}_{\nu,s'}(\mathbf{G}) = \sum_{\mathbf{G}'} \psi^{\Gamma}_{\nu,s'}(\mathbf{G}')\mathcal{S}_n(\mathbf{G}',\mathbf{G}) \tag{23}$$

and

$$\sum_{\mathbf{G}} [\psi^{\Gamma}_{\nu,s}(\mathbf{G})]^* T^{\Gamma}_{\nu,s'}(\mathbf{G}) = \mathrm{Re}\sum_{\mathbf{G}}^{h} [\psi^{\Gamma}_{\nu,s}(\mathbf{G})]^* T^{\Gamma}_{\nu,s'}(\mathbf{G})$$
$$= \mathrm{Re}\sum_{\Lambda}\sum_{\mathbf{G}}^{r} w(\mathbf{G})$$
$$\times [\psi^{\Gamma}_{\nu,s}(\Lambda\mathbf{G})]^* T^{\Gamma}_{\nu,s'}(\Lambda\mathbf{G}). \tag{24}$$

Due to point-group symmetry, we only have to evaluate $T^{\Gamma}_{\nu,s}(\mathbf{G})$ for $\mathbf{G}$ within the irreducible segment of the Brillouin zone, and the rest can be obtained via the symmetry transformation

$$T^{\Gamma}_{\nu,s}(\Lambda\mathbf{G}) = \sum_{\nu'} \Gamma_{\nu,\nu'}(\Lambda) T^{\Gamma}_{\nu,s}(\mathbf{G}). \tag{25}$$

Finally, we have

$$\sum_{\mathbf{G}} [\psi^{\Gamma}_{s}(\mathbf{G})]^* T^{\Gamma}_{s'}(\mathbf{G}) = \sum_{\nu'}\sum_{\mathbf{G}}^{r} [n(G^*)/n_{\Gamma}][\psi^{\Gamma}_{\nu',s}(\mathbf{G})]^* T^{\Gamma}_{\nu',s'}(\mathbf{G}). \tag{26}$$

The computation time of S and H scales according to N^2L for terms involving α and β and according to N^2M for other terms, where N denotes the total number of orbitals, L denotes the number of orbitals needed in the expansion between two different centers, and M denotes the number of G vectors needed to describe the Fourier transform of the wave function. With block diagonalization through symmetrization, the computation time is reduced by a factor $\sim n_h$. In addition the reduction from summation over the full $\mathbf{G}$ space to the summation over the irreducible segment leads to another factor $\sim n_h$. Thus, the total saving in computing S and H is a factor $\sim n_h^2$, which is quite significant for high-symmetry systems.

B. Effect of spin-orbit interaction

The inclusion of spin-orbit interaction typically takes much more computation effort, since the number of basis functions are doubled. In the LASTO code, the most time-consuming part occurs at the evaluation of the matrix elements of the spin-orbit term V_{so} between LASTO basis functions. Since V_{so}, which takes the form $(dV/dr)\mathbf{S}\cdot\mathbf{L}$, is appreciable only within the MT spheres, we have

$$\langle \psi_N \chi_\sigma | V_{so} | \psi_{N'} \chi_{\sigma'} \rangle = \sum_{\tilde{N}} \sum_{n=0,\pm 1} B_{NN'}(\tilde{N},n) \langle \tilde{l}\tilde{m}; 1/2, \sigma | \mathbf{S}\cdot\mathbf{L} | \tilde{l}\tilde{m} + n; 1/2, \sigma - n \rangle \delta_{\sigma,\sigma'+n}, \tag{27}$$

where χ_σ denotes the electron spinor with $\sigma = 1/2, -1/2$,

$$B_{NN'}(\tilde{N},n) \equiv \beta^*_{N\tilde{N}} \beta_{N'\tilde{N}+n} \Delta_{\tilde{l}} + \alpha^*_{N\tilde{N}} \alpha_{N'\tilde{N}+n} \dot{\Delta}_{\tilde{l}} + [\beta^*_{N\tilde{N}} \alpha_{N'\tilde{N}+n} + \alpha^*_{N\tilde{N}} \beta_{N'\tilde{N}+n}] \tilde{\Delta}_{\tilde{l}}. \tag{28}$$

Here $\tilde{N}+n$ is an abbreviation for $(\tilde{i},\tilde{l},\tilde{m}+n)$; $n=0,-1,1$ and $\langle \tilde{l}\tilde{m}; 1/2, \sigma | \mathbf{S}\cdot\mathbf{L} | \tilde{l}\tilde{m}+n; 1/2, \sigma - n \rangle$ denote the nonvanishing angular momentum coupling coefficients:

$$\Delta_l \equiv \int dr \frac{dV}{dr} |g_l(r)|^2, \tag{29}$$

$$\dot{\Delta}_l \equiv \int dr \frac{dV}{dr} |\dot{g}_l(r)|^2, \tag{30}$$

and

$$\tilde{\Delta}_l \equiv \int dr \frac{dV}{dr} g_l(r) \dot{g}_l(r). \tag{31}$$

For large supercells, the evaluation of this matrix plus the related steps to obtain the charge density (including the spin-orbit coupling) takes up about 90% of CPU time, since it scales like MN^3, where M is number of spherical harmonics used in the expansion divided by the number of basis functions per site and N is the total number of LASTO orbitals for the supercell. Fortunately, we can adopt the symmetrization procedure as described above with the use of double-group representations, and it reduces the CPU time by one order of magnitude for high-symmetry cases (such as T_d and D_{2d} point groups). Namely, we use the product of the symmetrized LASTO orbitals described above and the electron spinor χ to form symmetrized spin-orbit coupled basis functions that transform according to double-group representations of the point group. Within this symmetrized basis, the above V_{so} is block diagonalized with all Kramer's degenerate pairs being decoupled. For the T_d point group, the matrix is decomposed into eight diagonal blocks (two each for the Γ_6 and Γ_7 representations and four for the Γ_8 representation). Only three out of the eight blocks need to be evaluated, since degenerate states will lead to the same contribution to the total density. Thus we achieved a reduction of approximately 20-fold with this approach. For D_{2d} and C_{3v} groups the reduction is about eightfold and fourfold, respectively.

III. RESULTS AND DISCUSSIONS

To find the optimum values for the exponents (ζ) used in the LASTO basis functions for the present study, we first minimize the total energy of bulk CdTe and ZnTe against the variation of ζ values. The Hedin-Lundqvist exchange-correlation potential has been used. The MT sphere radius used is 2.59 a.u. for both Cd and Te and 2.4 a.u. for Zn. We use three ζ values for s-like and p-like orbitals and two ζ values for the d-like orbital of each atom. To improve the total energy, we put empty MT spheres with radius $r_s = 2.4$ a.u. at the interstitial sites. The optimized ζ values for the basis functions at interstitial sites are listed in the row labeled V in Table I. The lattice constants for CdTe and ZnTe obtained with the optimum set are 6.45 Å and 6.10 Å, re-

TABLE I. Optimized ζ values for Zn, Cd, Te, and Cl.

Cd :	ζ_{4s}=1.7, 1.3	ζ_{4p}=1.6, 1.2	ζ_{4d}=2.3
	ζ_{5s}=2.5	ζ_{5p}=2.5	ζ_{5d}=1.0
Zn :	ζ_{3s}=1.3, 0.9	ζ_{3p}=1.0, 0.6	ζ_{3d}=1.7
	ζ_{4s}=1.5	ζ_{4p}=1.4	ζ_{3d}=1.0
Te :	ζ_{4s}=1.7, 1.3	ζ_{4p}=1.6, 1.2	ζ_{5d}=1.2
	ζ_{4s}=2.1	ζ_{4p}=2.0	ζ_{5d}=0.5
V :	ζ_{1s}=1.6, 1.1	ζ_{2p}=1.5, 1.1	ζ_{3d}=1.4, 2.0
Cl :	ζ_{2s}=2.15, 1.7	ζ_{2p}=2.05, 1.6	ζ_{3d}=0.8

spectively, which are in close agreement with the low-temperature experimental values of 6.48 Å and 6.10 Å.[19] The band structures for CdTe and ZnTe calculated with these parameters with and without including the spin-orbit coupling self-consistently are shown as solid and dotted lines in Figs. 2 and 3, respectively. The calculated spin-orbit splitting for the valence bands at the zone center is 0.862 eV for CdTe and 0.888 eV for ZnTe, which agree well with the full potential LAPW results[13] and experimental values.[20,21]

We also calculate the cohesive energies by taking the difference in total energy between the bulk and isolated atoms (both with spin-orbit interaction). The cohesive energies obtained this way for CdTe and ZnTe are 4.05 eV and 4.30 eV, which are reasonably close to the corresponding experimental values (4.4 eV and 4.7 eV, respectively),[22] considering that we have used the local density approximation and a small set of basis functions. Note that the total energies of free atoms are also calculated within the LDA. It is known that the LDA tends to predict artificially lower total energies in comparison with the presumably more accurate generalized gradient approximation (GGA).[6,24] However, since we are taking the difference between two calculations both done within the LDA, the errors caused by the LDA tend to cancel out. Thus, the most significant error in the cohesive energy so calculated is likely due to the incompleteness of the basis used. The band gaps obtained (including spin-orbit interaction) are 0.25 and 0.72 eV for CdTe and ZnTe, respectively, which are lower than the experimental values of 1.6 and 2.2 eV considerably. This is a common problem with the LDA calculations.[23] This may cause serious error in the determination of the energy position of the defect levels, if the defect states contain strong admixture of the valence-band and conduction states. Fortunately, for CdTe and ZnTe, the defect states of interest are derived mostly from the valence band states. Thus, their energy positions relative to the valence-band maximum (VBM) may still be determined with reasonably accuracy, even though the band gaps are greatly underestimated. To examine the effect of number of **k** points used in the zone integration, we have compared results obtained with 60 special points and 10 special points within the irreducible segment of the fcc Brillouin zone by using the Monkhorst-Pack scheme.[25] It is worth noting that the bulk calculation with 10 special **k** points is equivalent to that of a 128-atom supercell calculation with one sampling point at $\mathbf{k}=0$. We found that the band gaps obtained in these two cases differ by 0.06 eV for CdTe and 0.15 eV for ZnTe, while the spin-orbit splittings obtained in these two cases are almost the same (with difference less than 0.01 eV). These differences indicate the size of error introduced by using the one-point sampling on the relative single-particle energy levels. Of course, the size of error can be reduced if a larger supercell is used. If we compare the total energies obtained in these two cases, we find a difference of 0.38 eV for CdTe and 0.50 eV for ZnTe. Thus, the total energy obtained by using a 128-atom supercell with $\mathbf{k}=0$ has a more noticeable error in absolute total energy. However, we expect such an error to be mostly cancelled out when we calculate the difference of two systems (e.g., one with vacancy and one without) by using the same size of supercell for both calculations.

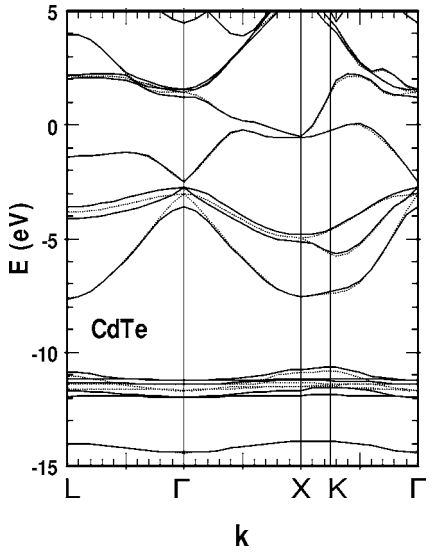

FIG. 2. Band structures of bulk CdTe obtained by the present full-potential method. Solid lines: with spin-orbit interaction. Dotted lines: without spin-orbit interaction.

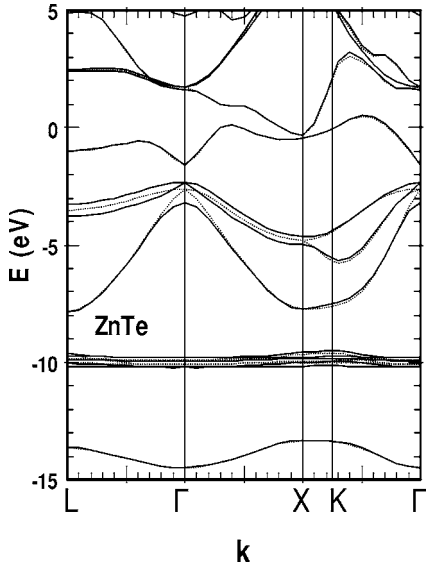

FIG. 3. Band structures of bulk ZnTe obtained by the present full-potential method. Solid lines: with spin-orbit interaction. Dotted lines: without spin-orbit interaction.

TABLE II. Relaxation parameters (δd_1 and δd_2) and energy lowered due to relaxation (ΔE) for neutral (V^0), singly charged (V^{-1}), and doubly charged (V^{-2}) Cd vacancies in CdTe calculated via 54- and 128- atom supercells. All energies are in eV. The values outside (inside) parentheses are results obtained with (without) the inclusion of the spin-orbit interaction.

N		V^0	V^{-1}	V^{-2}
54	δd_1	−0.091(−0.080)	−0.094(−0.091)	−0.094(−0.092)
	δd_2	−0.020(−0.019)	−0.022(−0.021)	−0.023(−0.022)
	ΔE	0.265 (0.112)	0.295 (0.254)	0.333 (0.346)
128	δd_1	−0.094(−0.084)	−0.094(−0.096)	−0.101(−0.097)
	δd_2	−0.021(−0.021)	−0.023(−0.023)	−0.026(−0.026)
	ΔE	0.318 (0.275)	0.371 (0.313)	0.411 (0.413)

A. Cd vacany in CdTe

We now minimize the total energy of a supercell system with a Cd vacancy at the center. We consider both the neutral and charged cases. The creation of a Cd vacancy generates four dangling bonds from the neighboring Te sites, which can accommodate eight electrons with six contributed from the neighboring Te atoms. Thus, it requires two additional electrons to fully occupy these four dangling bond, which renders the vacancy doubly charged. For neutral and singly charged vacancies, these dangling bonds are only partially occupied, which can lead to a possible Jahn-Teller distortion with either C_{3v} or D_{2d} symmetry.[18,26] We first consider the case with T_d symmetry for neutral and charged vacancies and later consider the possibility of Jahn-Teller distortion (for neutral and singly charged vacancy). The charge states are calculated by adding a uniform positively charged background, so the whole system remains charge neutral. This is a common practice used in all supercell simulation of defect levels. To reduce computation time for large supercell calculations, we use only two leading ζ values for s-like and p-like orbitals and one ζ value for the d-like orbital of each atom (as listed in the first row for each element in Table I). Furthermore, the basis function associated with empty spheres at interstitial sties is ignored. These additional orbitals were used in the bulk calculation in order to improve the accuracy on the predicted cohesive energy. However, they will not have a significant effect on the defect energy levels of interest here. On the vacancy site, we put an empty MT sphere with radius r_s=2.0 a.u. (for Cd) and 1.7 a.u. (for Zn). Five LASTO basis functions (two 1s like, two 2p like, and one 3d like) are used for the "vacancy" atom (denoted V). The 4 nearest-neighbor Te atoms and the 12 second-neighbor atoms surrounding the Cd vacancy are allowed to relax symmetrically toward the center. The fractional change of vacancy-Te distance (δd_1) and vacancy-Cd distance (δd_2) and the energy lowered due to relaxation (ΔE) for neutral (V^0), singly charged (V^{-1}), and doubly charged Cd vacancies (V^{-2}) in CdTe, calculated with supercells of 54 and 128 atoms, are listed in Table II. Results with and without a spin-orbit interaction are both presented. We find that the system is most stable (with minimum total energy) when the second-neighbor atoms contract slightly (about 2%) and the nearest-neighbor Te atoms contract about 10% toward the Cd vacancy site. The relaxed geometry is not very sensitive to the size of supercell used as long as it contains at least 54 atoms. The energy gained due to relaxation ranges between 0.1 and 0.4 eV, depending on the charge of the vacancy (with more negatively charged state having the lower energy).

TABLE III. Energies (relative to the valence-band maximum of bulk CdTe) of the defect-induced states for Cd vacancy in CdTe calculated via the use of a 128-atom supercell. The results obtained with the 54-atom supercell are also included in parentheses for comparison. All energies are in eV.

State	V^0	V^{-1}	V^{-2}
A_1	−1.438(−1.955)	−1.440(−1.922)	−1.287(−1.759)
T_2	0.068 (0.042)	0.099 (0.081)	0.201 (0.180)
Γ_6	−1.857(−2.328)	−1.815(−2.290)	−1.778(−2.219)
Γ_7	−0.460(−0.585)	−0.401(−0.522)	−0.306(−0.426)
Γ_8	0.049 (0.033)	0.067 (0.052)	0.111 (0.093)

The energies of the defect levels relative to the VBM of bulk CdTe for neutral and charged vacancies are listed in Table III. When the T_d symmetry is preserved, there are two defect levels, characterized by the Γ_1 (or A_1) and Γ_5 (or T_2) symmetry when the spin-orbit interaction is ignored. These levels are identified by examining their wave functions. The A_1 level lies inside the valence band (a resonance state), while the T_2 level lies above the valence-band maximum of bulk CdTe (in the band gap). Our result for the single-particle energy of the T_2 level (0.068 eV) for V^0_{Cd} is consistent with the result 0.06 eV obtained by the LAPW calculation.[13] We find significant differences between the results obtained from 54-atom and 128-atom supercells, especially for the A_1 level, which is about 0.5 eV too deep as predicted by the 54-atom supercell. Such a discrepancy is expected, since the resonance state is strongly mixed with the bulklike states and it has a large dispersion when the size of supercell is small. Namely, the intervacancy coupling is still quite sizable for the resonance states calculated by the 54-atom supercell. For the midgap states, the wave function is localized, and the difference becomes much smaller (less than 0.03 eV).

The modified Mulliken populations (as defined in Ref. 16) of the defect levels obtained from the 128-atom supercell are shown in Tables IV and V. Here shell (lmn) contains atomic site $(l,m,n)a/4$ and all other sites linked by the point-group operations. The shells with odd indices contain Te atoms, while those with even indices contain Cd atoms. The leading atom of each shell is within the irreducible segment of the Wigner-Seitz cell of the system and is indicated by a square (for cation) or circle (for anion) in Fig. 1. The population at the vacancy site is always less than 1% and is omitted here. For the T_2 level, the Mulliken population listed here contain predominantly Te p character with only less than 2% population in the s-like orbitals. This suggests that the T_2 level is mostly derived from the valence-band states, and the energy position relative to VBM as predicted here should not be influenced much by the many-body self-energy correction,[23,27] which may be added to get the band gap in

TABLE IV. Modified Mulliken populations of the defect-induced states for Cd vacancy in CdTe (without spin-orbit interaction).

	V^0		V^{-1}		V^{-2}	
Shell	A_1	T_2	A_1	T_2	A_1	T_2
(111)	0.628	0.326	0.629	0.382	0.643	0.480
(220)	0.073	0.030	0.074	0.039	0.087	0.058
(131)	0.008	0.137	0.008	0.122	0.003	0.086
(040)	0.004	0.001	0.004	0.001	0.003	0.001
(331)	0.200	0.258	0.200	0.261	0.184	0.258
(242)	0.014	0.004	0.014	0.005	0.013	0.005
$(\bar{2}\bar{4}\bar{2})$	0.009	0.004	0.010	0.004	0.010	0.005
(151)	0.008	0.058	0.008	0.039	0.006	0.014
(333)	0.002	0.024	0.002	0.018	0.001	0.009
(440)	0.020	0.006	0.020	0.006	0.018	0.017
(444)	0.000	0.001	0.000	0.000	0.000	0.000
$(\bar{4}\bar{4}\bar{4})$	0.000	0.000	0.000	0.001	0.000	0.001
(351)	0.012	0.077	0.012	0.060	0.011	0.033
(260)	0.002	0.001	0.002	0.001	0.001	0.000
(353)	0.018	0.058	0.018	0.053	0.017	0.022
(171)	0.001	0.014	0.001	0.008	0.001	0.003
(080)	0.000	0.000	0.000	0.000	0.000	0.000

close agreement with experiment. We find that all defect-induced midgap states are well localized within the first five shells except for the neutral vacancy, where about 20% population of the state falls outside the fifth shell.

TABLE V. Modified Mulliken populations of the defect-induced states for Cd vacancy in CdTe (with spin-orbit interaction).

	V^0			V^{-2}		
Shell	Γ_6	Γ_7	Γ_8	Γ_6	Γ_7	Γ_8
(111)	0.499	0.608	0.247	0.316	0.618	0.349
(220)	0.076	0.080	0.021	0.075	0.091	0.037
(131)	0.048	0.022	0.163	0.089	0.022	0.134
(040)	0.016	0.001	0.001	0.017	0.001	0.001
(331)	0.197	0.231	0.247	0.159	0.218	0.265
(242)	0.022	0.007	0.004	0.024	0.007	0.004
$(\bar{2}\bar{4}\bar{2})$	0.012	0.003	0.004	0.032	0.003	0.005
(151)	0.040	0.002	0.084	0.084	0.001	0.044
(333)	0.010	0.002	0.032	0.026	0.001	0.018
(440)	0.031	0.010	0.005	0.045	0.009	0.006
(444)	0.000	0.001	0.000	0.000	0.001	0.000
$(\bar{4}\bar{4}\bar{4})$	0.000	0.001	0.001	0.000	0.001	0.000
(351)	0.029	0.008	0.108	0.098	0.008	0.071
(260)	0.005	0.001	0.001	0.015	0.001	0.001
(353)	0.012	0.023	0.060	0.007	0.019	0.054
(171)	0.004	0.000	0.022	0.013	0.000	0.009
(080)	0.000	0.000	0.000	0.000	0.000	0.000

When the spin-orbit interaction is included, the A_1 level becomes a Γ_6 level (with twofold Kramers degeneracy), while the T_2 level splits into a twofold Γ_7 level and a fourfold Γ_8 level. Throughout the paper, we adopt the notation of Ref. 28 for the double-group representations. Their corresponding energies are listed in the lower half of Table III. The Γ_7 level moves into the valence-band, while the Γ_8 level remains in the gap (less than 0.1 eV above the valence-band maximum). This Γ_8 level will paly an important role in determining the capture cross section of holes in CdTe.

The T_2 level is fully occupied (with six electrons) for the doubly charged vacancy and partially occupied for singly charged and neutral vacancies, which may lead to a Jahn-Teller distortion. For neutral and singly charged vacancies, both trigonal (with C_{3v} symmetry) and tetragonal (with D_{2d} symmetry) Jahn-Teller distortions are considered. The starting positions of the four Te atoms are taken to be the relaxed atomic positions obtained above (which preserves the T_d symmetry). For the trigonal distortion, the Te atom along the [111] axis moves away from the center, while the other three Te atoms move toward the center. The change in vacancy-Te distance along [111] (δa) and for other three bonds (δb) is varied to minimize the total energy. For the tetragonal distortion, the two Te atoms at (1,1,1) and (−1,−1,1) sites move toward each other along the [110] direction, while the two Te atoms at (1,−1,−1) and (−1,1,−1) sites move toward each other along the [1-10] direction. A 54-atom supercell is used for this calculation, because the intervacancy distance is larger than that in the 64-atom supercell, and the reduction in symmetry requires much more computational effort, which makes the 128-atom supercell impractical to use. We find that for both neutral and singly charged vacancies the optimized geometry with T_d symmetry remains to be the most stable against either trigonal or tetragonal distortion.

For the neutral vacancy, we can estimate the formation energy for zero chemical potential by taking the difference in total energy between the supercell with a vacancy plus an isolated Cd atom and that without the vacancy (the bulk equivalent). We obtain a formation energy (including the spin-orbit interaction) of 2.79 eV (with 128-atom supercell) and 2.41 eV (with 54-atom supercell). This is compared with the result of 2.67 eV obtained by the LAPW method with 32-atom supercell and an energy cutoff of 8.5 Ry.[13]

B. Cd-vacancy—Cl pair in CdTe

The Cd vacancy is usually accompanied by a shallow halogen donor such as Cl in an *n*-type doped sample. Many experimental studies on the Cd-vacancy—Cl pair (also known as the *A* center) have been reported. Theoretically, only an empirical tight-binding study for the ideal configuration (and without the spin-orbit interaction) is available.[11] Here we calculate the electronic structures of the neutral ($[V-Cl]^0$) and singly charged Cd-vacancy—Cl pair ($[V-Cl]^-$) via the full-potential *ab initio* method with a 54-atom super-cell. In our calculation, we simply replace one Te atom next to the Cd vacancy by a Cl atom. The Cl and the three Te atoms are allowed to relax (with the three Te atoms assumed to move symmetrically along the direction of dan-

TABLE VI. Fraction change of distance from the vacancy site for the first five shells [$\delta d(lmn)$] for defect complexes $[\text{V-Cl}]^0$ and $[\text{V-Cl}]^-$ in CdTe calculated via a 54-atom supercell. The relaxation parameter for the fifth shell [$\delta d(0\bar{2}\bar{2})$] is assumed to be the same as that for the fourth shell [$\delta d(0\bar{2}2)$]. The energy lowered due to relaxation, ΔE (in eV), is also shown. The values outside (inside) parentheses are results obtained with (without) the inclusion of the spin-orbit interaction.

Complex	$\delta d(111)$	$\delta d(1\bar{1}\bar{1})$	$\delta d(022)$	$\delta d(0\bar{2}2)$	ΔE
$[\text{V-Cl}]^0$	0.206	−0.085	0.010	−0.020	0.332
	(0.200)	(−0.076)	(0.010)	(−0.018)	(0.318)
$[\text{V-Cl}]^-$	0.198	−0.085	0.010	−0.020	0.374
	(0.200)	(−0.074)	(0.012)	(−0.020)	(0.393)

gling bonds). The ζ values for Cl are determined by minimizing the total energy of a AgCl crystal with the same lattice structure as CdTe. Note that Ag has the same core as Cd, so the ζ values for Ag are assumed to be the same as Cd. The optimized ζ values are listed in Table I. Note that two $2s$-like and two $2p$-like orbitals are used to describe the $3s$ and $3p$ orbitals of Cl for the same reason as discussed above for CdTe. Minimization of the total energy reveals that the three Te atoms move toward the Cd vacancy by 8% and the Cl atom move away from the vacancy by 20% for both neutral and charged cases (with the second-neighbor atoms surrounding the three Te atoms relaxing inward by 2%). With this relaxation the energy is lowered by 0.33 eV and 0.37 eV (relative to the ideal geometry) for $[\text{V}-\text{Cl}]^0$ and $[\text{V}-\text{Cl}]^{-1}$, respectively. The details of the relaxation parameters and energy gained due to relation for $[\text{V}-\text{Cl}]^0$ and $[\text{V}-\text{Cl}]^{-1}$ are given in Table VI. The formation energy of $[\text{V}-\text{Cl}]^0$ is found to be 1.74 eV. This is lower than the formation energy of V_{Cd}^0, indicating the tendency to form a vacancy-Cl complex when the Cl dopant is present. The energies of the defect levels are identified by examining the wave functions. Two defect levels with A_1 and E symmetry are found. They are mainly derived from the three dangling bonds associated with the Te atoms surrounding the vacancy. The energy positions relative to the bulk valence-band maximum for these defect levels and the corresponding modified Mulliken populations are listed in Table VII. The A_1 level is below the bulk valence-band maximum, while the twofold E level fall into the band gap. Assuming that the finite-size effect on the A_1 level is similar to the case for Cd vacancy, then the energy positions for A_1 levels obtained by the 54-atom supercell should be shifted up by about 0.5 eV. The E-symmetry level here corresponds to the T_2 level of the Cd vacancy discussed above, so it is much less affected by the finite size of the supercell. When the spin-orbit interaction is included, the twofold E-symmetry level (which is fourfold with spin) splits into a Γ_4 and Γ_5 level (both with twofold Kramers degeneracy). Their energy positions relative to the bulk valence-band maximum and the corresponding modified Mulliken populations are listed in Table VIII. We note that for $[\text{V-Cl}]^0$, both of these levels move into the valence band, while for $[\text{V-Cl}]^{-1}$, one level (with Γ_5 symmetry) remains above the valence-band maximum by about 0.05 eV.

Experimental studies on charged Cd vacancy levels are still inconclusive. Many levels in the fundamental gap of CdTe have been reported, but they have not been associated with a specific vacancy. Most experimental studies indicate these midgap states are associated with defect complexes. For Cl-doped CdTe samples, a zero-phonon line at 1.473 eV was observed in the recombination luminescence, which suggests that the defect level lies around 0.12 eV above the valence-band maximum.[9] Thus, our theoretical prediction for the Γ_5-symmetry level of $[\text{V-Cl}]^{-1}$ (which lies at 0.05 eV above the VBM) is in reasonable agreement with this observation, considering that the uncertainty of our theoretical

TABLE VII. Modified Mulliken populations of the defect-induced states for the Cd-vacancy—Cl pair in CdTe (without spin-orbit interaction). The energies (in eV) of the defect levels relative to the bulk valence-band maximum are given in the parentheses following the symmetry label.

	$[\text{V-Cl}]^0$		$[\text{V-Cl}]^-$	
Shell	A_1 (−1.479)	E (0.046)	A_1 (−1.349)	E (0.160)
(111)	0.030	0.045	0.012	0.004
$(1\bar{1}\bar{1})$	0.383	0.421	0.512	0.544
(022)	0.016	0.005	0.008	0.005
$(0\bar{2}2)$	0.089	0.032	0.118	0.048
$(0\bar{2}\bar{2})$	0.010	0.148	0.012	0.023
$(\bar{3}\bar{1}\bar{1})$	0.057	0.434	0.040	0.015
$(\bar{3}11)$	0.037	0.092	0.041	0.018
$(3\bar{1}1)$	0.085	0.042	0.063	0.000
(004)	0.000	0.000	0.006	0.001
$(00\bar{4})$	0.014	0.001	0.010	0.066
$(1\bar{3}\bar{3})$	0.059	0.091	0.047	0.201
$(\bar{1}\bar{3}3)$	0.020	0.194	0.026	0.000
$(\bar{4}\bar{2}\bar{2})$	0.001	0.001	0.001	0.000
$(\bar{4}\bar{2}2)$	0.003	0.003	0.009	0.003
$(\bar{4}22)$	0.022	0.001	0.006	0.001
$(42\bar{2})$	0.024	0.000	0.014	0.000
$(\bar{5}\bar{1}1)$	0.024	0.040	0.009	0.012
$(5\bar{1}\bar{1})$	0.007	0.006	0.002	0.002
$(\bar{3}\bar{3}\bar{3})$	0.116	0.008	0.065	0.002

TABLE VIII. Modified Mulliken populations of the defect-induced states for the Cd-vacancy—Cl pair in CdTe (with spin-orbit interaction). The energies (in eV) of the defect levels relative to the bulk valence-band maximum are given in the parentheses following the symmetry label.

Shell	$[V-Cl]^0$		$[V-Cl]^-$	
	Γ_4 (−0.125)	Γ_5 (−0.017)	Γ_4 (−0.119)	Γ_5 (0.053)
(111)	0.006	0.004	0.006	0.003
$(1\bar{1}\bar{1})$	0.178	0.356	0.268	0.436
(022)	0.009	0.006	0.012	0.005
$(0\bar{2}2)$	0.013	0.027	0.022	0.035
$(0\bar{2}\bar{2})$	0.005	0.012	0.010	0.017
$(\bar{3}\bar{1}\bar{1})$	0.108	0.054	0.089	0.032
$(\bar{3}11)$	0.109	0.119	0.095	0.105
$(3\bar{1}1)$	0.186	0.053	0.154	0.035
(004)	0.002	0.000	0.001	0.000
$(00\bar{4})$	0.003	0.001	0.003	0.001
$(1\bar{3}\bar{3})$	0.079	0.093	0.081	0.074
$(\bar{1}\bar{3}3)$	0.128	0.199	0.142	0.212
$(\bar{4}\bar{2}\bar{2})$	0.001	0.001	0.001	0.001
$(\bar{4}\bar{2}2)$	0.004	0.003	0.004	0.003
$(\bar{4}22)$	0.001	0.002	0.001	0.002
$(42\bar{2})$	0.004	0.000	0.005	0.000
$(\bar{5}\bar{1}1)$	0.099	0.052	0.071	0.029
$(5\bar{1}\bar{1})$	0.030	0.009	0.022	0.004
$(\bar{3}\bar{3}\bar{3})$	0.035	0.010	0.024	0.005

procedure for determining the defect level is on the order of 0.1 eV.

C. Zn vacancy in ZnTe

The behavior of Zn vacancies in ZnTe is similar to that of Cd vacancies in CdTe. The main difference here is that the Zn atom is much smaller than Cd; thus, the degree of relaxation is much reduced. Relaxation parameters (δd_1 and δd_2) and energy lowered due to relaxation (ΔE) for neutral (V^0), singly charged (V^{-1}) and doubly charged (V^{-2}) Zn vacancies in ZnTe with Td symmetry are shown in Table IX. Because the second-neighbor Zn atoms surrounding the vacancy site have a tendency to contract more than the first-neighbor Te atoms, here we need to use a slightly smaller radius (2.31 a.u.) for Zn MT spheres in order to leave enough room for the relaxation. The formation energy for neutral vacancy is found to 2.83 eV (with 128-atom supercell) and 2.34 eV (with 54-atom supercell). We have also studied the possible Jahn-Teller distortion for neutral and singly charged Zn vacancies in ZnTe, and again we find that the geometry with T_d symmetry remains to be the most stable against either trigonal or tetragonal distortion. Energies (relative to the valence-band maximum of bulk CdTe) of the defect-induced states for Zn vacancies in ZnTe calculated via the use of 54- and 128-atom supercells are listed in Table X. Comparing Table X with Table III for Cd vacancies, we note that the energies of defect levels for Zn vacancies are consistently higher than the corresponding Cd vacancies by approximately 0.05 eV. This allows us to provide a rough estimate of the energy position of cation vacancy level in CdZnTe via a linear interpolation scheme. For example, our calculation predicts that the energy level of the doubly charged cation vacancy to increase by about 12 meV (relative to VBM) from CdTe to $Cd_{0.8}Zn_{0.2}Te$.

TABLE IX. Relaxation parameters (δd_1 and δd_2) and energy lowered due to relaxation (ΔE) for neutral (V^0), singly charged (V^{-1}), and doubly charged (V^{-2}) Zn vacancies in ZnTe calculated via a 128-atom supercell. All energies are in eV. The values outside (inside) parentheses are results obtained with (without) the inclusion of spin-orbit interaction.

N		V^0	V^{-1}	V^{-2}
54	δd_1	0.000 (0.009)	−0.003 (0.000)	−0.023(−0.011)
	δd_2	−0.005(−0.004)	−0.006(−0.006)	−0.010(−0.006)
	ΔE	0.035 (0.029)	0.049 (0.044)	0.095 (0.068)
128	δd_1	−0.030(−0.025)	−0.030(−0.030)	−0.043(−0.039)
	δd_2	−0.012(−0.010)	−0.014(−0.012)	−0.017(−0.016)
	ΔE	0.090 (0.067)	0.129 (0.092)	0.167 (0.166)

IV. SUMMARY

We have implemented a symmetrized basis scheme for the linearized augmented Slater-type orbital method, which allows efficient calculation of a system with large unit cell with high symmetry. This approach reduces the memory requirement by one order of magnitude and the computation time by two orders of magnitude. We have applied this method to calculate various charged states of Cd vacancy and vacancy-Cl pair in CdTe and ZnTe. The atomic relaxation and effect of spin-orbit interaction are properly taken into account. The relaxation of atoms surrounding the defect, the formation energy, and energy levels of defect-induced states are calculated. It is found that the relaxed geometry for

TABLE X. Energies (relative to the valence-band maximum of bulk ZnTe) of the defect-induced states for Zn vacancy in ZnTe calculated via the use of a 128-atom supercell. The results obtained with the 54-atom supercell are also included in parentheses for comparison. All energies are in eV.

State	V^0	V^{-1}	V^{-2}
Γ_1	−1.485(−1.884)	−1.399(−1.770)	−1.255(−1.634)
Γ_5	0.087 (0.102)	0.149 (0.185)	0.290 (0.341)
Γ_6	−1.667(−2.120)	−1.640(−2.130)	−1.586(−2.009)
Γ_7	−0.421(−0.430)	−0.347(−0.386)	−0.220(−0.191)
Γ_8	0.073 (0.114)	0.102 (0.136)	0.173 (0.264)

these defects are rather insensitive to the size of supercell used, as long as it is larger than 54 atoms, while the energy levels of the defect-induced states are somewhat sensitive to the size of the supercell. We determine the energy position of the defect levels for systems with T_d symmetry via a 128-atom supercell and that with C3v symmetry via a 54-atom supercell. We find a defect level in the band gap with an energy above the valence-band maximum by about 0.03–0.1 eV for Cd vacancies in CdTe and 0.1–0.2 eV for Zn vacancies in ZnTe. We also examined the possibility of Jahn-Teller distortion for neutral and singly charged vacancies in CdTe and ZnTe with the use of a 54-atom supercell. We find that the system with T_d symmetry remains stable against either trigonal or tetragonal distortion. The results presented in the paper can be affected by the following. First, we cannot rule out the possibility of a Jahn-Teller distortion in the charge states when an even larger supercell is used and atoms are allowed to relax beyond the third-neighbor distance. Second, the self-energy correction due to many-body effects should be considered in order to obtain reliable defect level energies, although for states derived mostly from valence bands such an effect is likely to be small. Finally, the introduction of a uniform positively charged background may not represent the realistic situation accurately and it can lead to errors in the predicted positions of defect levels relative to the valence-band maximum. Such a constraint can be removed in a Green's function approach with a large perturbation domain. The implementation of such a scheme can be done with the LASTO basis functions by carrying out the computation of matrix elements all in real space and will be considered in the future.

ACKNOWLEDGMENTS

The author would like to thank Jincheng Zheng for fruitful discussions. This work was supported in part by the Department of Energy under Contract No. DE-AC02-98CH1-886 and by an ARO MURI program under Contract No. DAAD19-01-1-0591.

APPENDIX: SYMMETRIZATION COEFFICIENTS

To obtain the symmetrization coefficients $C(i,lm)$, we first construct the lattice harmonics at each site j. The lattice harmonics is the linear combination of spherical harmonics of the same l that transforms like a basis function (labeled ν) associated with an irreducible representation (labeled Γ) of a point group. We define

$$K_l^{\Gamma\nu}(\mathbf{G}) = \sum_m C_{lm}^{\Gamma\nu} Y_{lm}(\mathbf{G}). \tag{A1}$$

In general, these coefficients can be obtained via the use of projection operator. We have

$$C_{lm}^{\Gamma\nu} = \frac{n(\Gamma)}{h} \sum_\Lambda \Gamma_{\nu,\nu}(\Lambda) \mathcal{D}_{m,m'}^{(l)}(\Lambda), \tag{A2}$$

where $n(\Gamma)$ is the dimension of irreducible representation Γ, h is the order of the point group, Λ denotes a group operation, and $\mathcal{D}_{m,m'}^{(l)}(\Lambda) \equiv \int d\Omega Y_{lm}^*(\Omega) Y_{lm'}(\Lambda^{-1}\Omega)$, which can be evaluated efficiently via the Gaussian quadrature method.

Next we construct the symmetrized site functions for each shell s defined as

$$S_s^{\Gamma\nu} = \sum_m C_s^{\Gamma\nu}(j) e^{i\mathbf{G}\cdot\mathbf{r}_j}. \tag{A3}$$

Using the projection operator, we obtain

$$C_s^{\Gamma\nu}(j) = \frac{n(\Gamma)}{h} \sum_\Lambda \Gamma_{\nu,\nu}(\Lambda) \mathcal{D}_{j,j'}^{(s)}(\Lambda), \tag{A4}$$

where $\mathcal{D}_{j,j'}^{(s)}(\Lambda) \equiv \Sigma_{\mathbf{G}} e^{i\mathbf{G}\cdot(\mathbf{r}_j - \Lambda^{-1}\mathbf{r}_{j'})}$ which is 1 if $(\mathbf{r}_j - \Lambda^{-1}\mathbf{r}_{j'})$ is a lattice vector of the "superlattice" and zero otherwise. Finally, we use the direct products of cubic harmonics and the symmetrized site functions to obtain the fully symmetrized states. We have

$$\psi_{ls}^{\Gamma\mu} = \sum_{\gamma\nu,\gamma'\nu'} V_\mu^\Gamma(\gamma\nu,\gamma'\nu') K_l^{\gamma\nu} S_s^{\gamma'\nu'}, \tag{A5}$$

where $V_\mu^\Gamma(\gamma\nu,\gamma'\nu')$ are the vector coupling coefficients, which are readily available in Ref. 28.

[1] See, for example, *Semiconductors for Room-Temperature Nuclear Detector Applications II*, edited by R. B. James, T. E. Schlesinger, P. Siffert, W. Dusi, M. Squillante, M. O'Connell, and M. Cuzin, MRS Symposic Proceedings No. 487 (Materials Research Society, Pittsburgh, 1998).
[2] T. Takebe, J. Saraie, and H. Matsunami, J. Appl. Phys. **53**, 457 (1982).
[3] L. C. Isett and Pr. K. Raychaudhuri, J. Appl. Phys. **55**, 3605 (1982).
[4] B. K. Meyer, W. Staler, D. M. Hofmann, P. Omling, D. Sinerius, and K. W. Benz, J. Cryst. Growth **117**, 656 (1992)
[5] L. Worschech, W. Ossau, F. Fischer, A. Waag, and G. Landwehr, J. Cryst. Growth **161**, 134 (1996).
[6] M. A. Berding, A. Sher, and M. van Schilfgaarde, J. Electron. Mater. **24**, 1127 (1995).
[7] M. A. Berding, Phys. Rev. B **60**, 8943 (1999).
[8] H. Shin and C. Sun, J. Cryst. Growth **186**, 354 (1998).
[9] D. M. Hofmann, P. Omling, H. G. Grimmeiss, B. K. Meyer, K. W. Benz, and D. Sinerius, Phys. Rev. B **45**, 6247 (1992).
[10] M. Hage-Ali and P. Siffert, Nucl. Instrum. Methods Phys. Res. A **322**, 313 (1992).
[11] P. H. E. Meijer, P. Pecheur, and G. Toussaint, Phys. Status Solidi B **140**, 155 (1987).
[12] S. Biernacki, U. Scherz, and B. K. Meyer, Phys. Rev. B **48**, 11726 (1993).
[13] S. H. Wei and S. B Zhang, Phys. Rev. B **66**, 155211 (2002).
[14] J. W. Davenport, Phys. Rev. B **29**, 2896 (1984).
[15] J. W. Davenport, M. Weinert, and R. E. Watson, Phys. Rev. B **32**,

4876 (1985).
[16] J. W. Davenport, R. E. Watson, and M. Weinert, Phys. Rev. B **32**, 4883 (1985).
[17] G. W. Fernando, J. W. Davenport, R. E. Watson, and M. Weinert, Phys. Rev. B **40**, 2757 (1989).
[18] M. J. Kirton, P. W. Bank, L. D. Lian, and M. Jaros, J. Phys. C **17**, 2487 (1984).
[19] *Physics of II-VI and I-VII Compounds*, edited by. Modelung, Landolt-Börnstein, New Series, Vol. 17, Pt. b (Springer-Verlag, Berlin, 1982).
[20] D. J. Chadi, J. P. Walter, M. L. Cohen, Y. Petroff, and M. Balkanski, Phys. Rev. B **5**, 3058 (1972).
[21] B. Segall and D. T. F. Marple, in *Physics and Chemistry of II-VI Compounds*, edited by M. Aven and J. S. Prener (North-Holland, Amsterdam, 1967), p. 319.
[22] T. Soma, J. Phys. C **11**, 2669 (1978).
[23] S. G. Louie, S. Froyen, and M. L. Cohen, Phys. Rev. B **26**, 1738 (1982).
[24] K. Carling, G. Wahnstrom, T. R. Mattsson, A. E. Mattsson, N. Sandberg, and G. Grimvall, Phys. Rev. Lett. **85**, 3862 (2000).
[25] H. J. Monkhorst and J. D. Pack, Phys. Rev. B **13**, 5188 (1976).
[26] G. Bevilacqua, L. Martinelli, and E. E. Vogel, Phys. Rev. B **66**, 155338 (2002), and references therein.
[27] N. E. Christensen, Phys. Rev. B **30**, 5753 (1984).
[28] G. F. Koster, J. O. Dimmock, R. G. Wheeler, and H. Statz, *Properties of the Thirty-Two Point Groups* (MIT Press, Cambridge, MA, 1963).